

A novel interconnection of Dynamic Movement Primitives (DMP) with a modified low impedance controlled robot for accurate tracking and compliant robot reactions

Konstantinos Vlachos, Zoe Doulgeri

Abstract—In this paper, a novel control scheme is proposed interconnecting a Dynamic Movement Primitives (DMP) system with a modified low impedance controlled robot to achieve compliance to unexpected contact events and high tracking accuracy under the presence of model and task uncertainties. The proposed control scheme is formulated in the joint space and theoretically shown to accurately track the desired trajectory under the presence of uncertainties. Simulations of 2-DOF manipulator model carrying an unknown load under the proposed scheme demonstrate its high tracking accuracy as compared to the low impedance controlled robot while exhibiting highly compliant reactions to external contact forces.

I. INTRODUCTION

Collaborative robots (Cobots) constitute a class of complex nonlinear dynamical systems that challenge traditional control approaches. The increasing incorporation of Cobots into dynamic and uncertain environments which require precision, adaptability and provable safety has established them as a critical testbed for advancing modern control theory. In dynamic and uncertain environments ensuring robotic safety is a major issue especially in cases where physical contact of the robot with a human or its environment in general cannot be entirely avoided. To address this safety issue, active compliance control approaches (impedance control, admittance control) have been proposed in the literature to realize a mass-spring-damper behavior between external wrenches and the resulting tracking error. By selecting low stiffness and damping the robot is able to modify its nominal trajectory to comply with external contact forces possibly arising in case of unexpected collisions with a human. However, a highly compliant behavior increases the effect of model and task uncertainties (i.e. addition of an extra load on the robot end-effector), which act as disturbances on the control system, compromising the tracking accuracy and establishing the well-known trade-off between compliance and accuracy in impedance control approaches [1].

Traditional control approaches such as Adaptive Control, Robust control and Proportional Integral Derivative (PID) control have demonstrated high tracking accuracy under model and task uncertainties but at the expense of the system's compliance to external contact forces [2] which makes them an unsuitable choice for collaborative robot applications.

This work has received funding from the European Union's Horizon Framework Programme for Research and Innovation under grant agreement no 101120823, project MANiBOT.

Obstacle avoidance methods is a popular approach for ensuring safety in robotic applications and they have been widely used in the literature. In [3] a prescribed performance like approach has been proposed which provides obstacle avoidance guarantees while in [4] Control Barrier Functions (CBF) are utilized to guarantee that the system remains inside a safe predefined set at all times. However, determining a safety set apriori in a dynamic and uncertain environment is not always a viable option. In general, such approaches assume an ideal perception system without errors or delays which is not the case in real world applications implying that even though the risk of an unexpected collision can be reduced it cannot be completely eliminated.

Variable impedance control approaches have been proposed in the literature to achieve high tracking accuracy and safety at the same time [5]. They utilize a highly stiff robot to achieve high tracking accuracy under model and task uncertainties and a stiffness adaptation law to drop the stiffness in case contact is detected. As these approaches operate in an inherently unsafe mode of operation (high stiffness) any delays in the perception of contact could jeopardize safety for both the human and the robot. In most cases these approaches require energy tanks to ensure the system's passivity during impedance regulation which fail if the energy tank is depleted [6].

Our previously published works [7], [8] achieve accuracy only in Cartesian position tracking in the presence of model and task uncertainties as well as compliant reactions to external forces given a linear and decoupled low Cartesian impedance for the robot control system. However, not guaranteeing tracking accuracy in orientation, limits the practicality of the approach in many applications. Moreover, the implementation of a linear and decoupled low impedance dynamics, requires external force measurements that introduce additional sources of error and delays into the control loop, which can affect the overall system performance.

In this work a novel interconnection of a DMP with a modified low impedance controlled robot which does not require inertia shaping is formulated in the joint space of the robot. It achieves high tracking accuracy and compliant robot reactions under the presence of model and task uncertainties for both position and orientation trajectories as opposed to our previous works [7], [8]. Eliminating the need for inertia shaping also removes the reliance on external force measurements, thereby reducing sensor requirements, eliminating additional errors and delays and simplifying the control

architecture. The stability and robustness of the proposed control scheme is proven with formal Lyapunov arguments. The theoretical results are validated via simulations on a 2-dof planar robot manipulator.

II. PRELIMINARIES

A. Dynamic Movement primitives

DMP have been proposed in the literature [9] for encoding complex motion trajectories derived via demonstrations while they are robust to target perturbations and enable motion trajectory modifications based on sensory feedback. In this work we utilize a DMP formulation proposed in [10] which enables forward and backward execution of the encoded motion trajectory. For simplicity and without loss of generality we shall present the 1-dof case. The DMP system is given by:

$$\begin{aligned} \ddot{q}_r &= \ddot{q}_x - d(\dot{q}_r - \dot{q}_x) - k(q_r - q_x) \\ \dot{x} &= \begin{cases} 1/\tau, & x < 1 \\ 0, & \text{otherwise} \end{cases}, \quad x(t_0) = 0 \end{aligned} \quad (1)$$

where $q_r, \dot{q}_r, \ddot{q}_r \in \mathbb{R}$ are the reference joint position, velocity and acceleration, k, d are positive scalars usually selected for critically damped response, x is a phase variable representing the time evolution of the desired joint trajectory q_x with τ being its total duration, which is given by:

$$\begin{aligned} q_x &= k_s(f(x) - f(x_0)) + q_0 \\ \dot{q}_x &= k_s \dot{f}_q(x) \\ \ddot{q}_x &= k_s \ddot{f}_q(x) \\ k_s &= (q_f - q_0)/(f(x_f) - f(x_0)) \\ f(x) &= \psi(x)^T \mathbf{w} \end{aligned} \quad (2)$$

where $q_0, q_f \in \mathbb{R}$ are the initial and goal joint position of the trajectory, k_s is the spatial scaling term, $f(x)$ encodes the demonstrated joint trajectory through a weighed sum of Gaussians where $\psi(x)^T = [\psi_1(x), \dots, \psi_N(x)]/\sum_{i=1}^N \psi_i(x)$ with $\psi_i(x) = \exp(-h_i(x - c_i)^2)$ being a Gaussian kernel with center c_i and inverse variance h_i , N is the total number of kernels and $\mathbf{w} = [w_1, \dots, w_N]$ is the weight vector. The weights are learned using joint position data via Least squares (LS) or Locally Weighed Regression (LWR) as in [10] and $\dot{f}(x), \ddot{f}(x)$ are derived through analytical derivation of $f(x)$.

B. Impedance Control

Consider an n-dof robot manipulator with its dynamics given by:

$$\mathbf{M}(\mathbf{q})\ddot{\mathbf{q}} + \mathbf{C}(\mathbf{q}, \dot{\mathbf{q}})\dot{\mathbf{q}} + \mathbf{g}(\mathbf{q}) = \boldsymbol{\tau}_c + \boldsymbol{\tau}_{cont} \quad (3)$$

where $\mathbf{q}, \dot{\mathbf{q}}, \ddot{\mathbf{q}} \in \mathbb{R}^n$ are the robot's joint positions, velocities and accelerations, $\mathbf{M}(\mathbf{q}), \mathbf{C}(\mathbf{q}, \dot{\mathbf{q}}) \in \mathbb{R}^{n \times n}$ and $\mathbf{g}(\mathbf{q}) \in \mathbb{R}^n$ are the mass matrix, the centrifugal/Coriolis matrix and the gravity vector respectively, $\boldsymbol{\tau}_c \in \mathbb{R}^n$ is the control input and $\boldsymbol{\tau}_{cont} \in \mathbb{R}^n$ are external contact torques arising from intentional or unintentional human-robot contact. Consider a desired trajectory given in terms of $\mathbf{q}_x, \dot{\mathbf{q}}_x, \ddot{\mathbf{q}}_x \in \mathbb{R}^n$ and

an estimation of the robot's dynamic model $\hat{\mathbf{M}}(\mathbf{q}), \hat{\mathbf{C}}(\mathbf{q}, \dot{\mathbf{q}}), \hat{\mathbf{g}}(\mathbf{q})$. Utilizing the following control input:

$$\boldsymbol{\tau}_c = \hat{\mathbf{M}}(\mathbf{q})\ddot{\mathbf{q}}_x + \hat{\mathbf{C}}(\mathbf{q}, \dot{\mathbf{q}})\dot{\mathbf{q}}_x + \hat{\mathbf{g}}(\mathbf{q}) - \mathbf{D}_d\dot{\tilde{\mathbf{q}}} - \mathbf{K}_d\tilde{\mathbf{q}} \quad (4)$$

where $\tilde{\mathbf{q}} = \mathbf{q} - \mathbf{q}_x$ is the tracking error and $\mathbf{K}_d, \mathbf{D}_d > 0$ are the desired stiffness and damping matrices respectively, yields the closed loop impedance dynamics:

$$\mathbf{M}(\mathbf{q})\ddot{\tilde{\mathbf{q}}} + (\mathbf{C}(\mathbf{q}, \dot{\mathbf{q}}) + \mathbf{D}_d)\dot{\tilde{\mathbf{q}}} + \mathbf{K}_d\tilde{\mathbf{q}} = \boldsymbol{\tau}_{dist} \quad (5)$$

where $\boldsymbol{\tau}_{dist} = \boldsymbol{\tau}_e + \boldsymbol{\tau}_{cont} \in \mathbb{R}^n$ is a disturbance input consisting of external contact torques $\boldsymbol{\tau}_{cont}$ and a disturbance input which arises due to estimation errors on the robot dynamic model $\boldsymbol{\tau}_e(\mathbf{q}, \dot{\mathbf{q}}, \ddot{\mathbf{q}}_x)$. This robot control system is known as impedance control without inertia shaping [1], realizing a non-linear mass-spring-damper behavior between the input $\boldsymbol{\tau}_{dist}$ and the resulting tracking error $\tilde{\mathbf{q}}$. This type of impedance control is computationally lighter and less sensitive to modeling errors compared to the inertia shaping approach since it does not require external torque measurements [1]. By selecting low stiffness and damping gains the system exhibits highly compliant reactions to external contact torques $\boldsymbol{\tau}_{cont}$ at the expense of larger tracking errors in the presence of model and task uncertainties $\boldsymbol{\tau}_e$.

III. PROPOSED CONTROL SCHEME

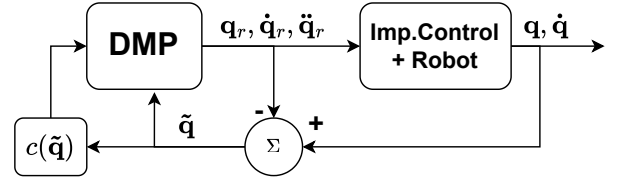


Fig. 1. Proposed control structure

The proposed control scheme consists of a DMP system which has encoded the desired joint trajectory coupled with the robot control system and is shown in Fig.1. The DMP system is based in (1) and expanded by a coupling term:

$$\begin{aligned} \ddot{q}_r &= \ddot{q}_x - d(\dot{q}_r - \dot{q}_x) - k(q_r - q_x) - kc(\|\tilde{\mathbf{q}}\|)\tilde{\mathbf{q}} \\ \dot{x} &= \begin{cases} 1/\tau(\|\tilde{\mathbf{q}}\|), & x < 1 \\ 0, & \text{otherwise} \end{cases}, \quad x(t_0) = 0 \end{aligned} \quad (6)$$

where $\mathbf{q}_x, \dot{\mathbf{q}}_x, \ddot{\mathbf{q}}_x \in \mathbb{R}^n$ is the desired motion trajectory given by (2) for each dof, $\tilde{\mathbf{q}} = \mathbf{q} - \mathbf{q}_r \in \mathbb{R}^n$ is a virtual tracking error with \mathbf{q} being the actual robot joint positions and \mathbf{q}_r being the reference joint positions generated by (6), k is the same gain parameter as in eq. (1) and $c : \mathbb{R} \rightarrow [0, 1]$ is a sigmoid like function given by:

$$c(\|\tilde{\mathbf{q}}\|) = \begin{cases} 1, & \|\tilde{\mathbf{q}}\| < \bar{e} \\ \exp(-\gamma_s(\|\tilde{\mathbf{q}}\| - \bar{e})^2), & \text{otherwise} \end{cases} \quad (7)$$

where γ_s is a positive scalar and \bar{e} a predefined upper bound of the virtual tracking error $\tilde{\mathbf{q}}$. Notice that we refer to $\tilde{\mathbf{q}} = \mathbf{q} - \mathbf{q}_r$ as the virtual tracking error since it is defined with respect to the reference trajectory \mathbf{q}_r and not with respect to the desired trajectory \mathbf{q}_x .

The total duration of the desired trajectory is adapted according to:

$$\tau(\|\tilde{\mathbf{q}}\|) = \frac{\tau_d}{c(\|\tilde{\mathbf{q}}\|)} \quad (8)$$

with τ_d being the target duration of the desired trajectory. The reference trajectory \mathbf{q}_r , $\dot{\mathbf{q}}_r$, $\ddot{\mathbf{q}}_r$ of (6) is fed to the robot controller utilizing a novel impedance-like control law which endows the closed-loop impedance dynamics with exponential convergence properties and it is given by:

$$\begin{aligned} \tau_c = & \hat{\mathbf{M}}(\mathbf{q})\ddot{\mathbf{q}}_r + \hat{\mathbf{C}}(\mathbf{q}, \dot{\mathbf{q}})(\dot{\mathbf{q}}_r - \mu\tilde{\mathbf{q}}) - (\mu\hat{\mathbf{M}}(\mathbf{q}) + \mathbf{D}_d)\dot{\tilde{\mathbf{q}}} \\ & - (\mu\mathbf{D}_d + \mathbf{K}_d)\tilde{\mathbf{q}} + \mathbf{g}(\mathbf{q}) \end{aligned} \quad (9)$$

with μ being some positive scalar. By applying input (9) to the robot dynamics (3) we get the following closed loop dynamics:

$$\begin{aligned} \mathbf{M}(\mathbf{q})\ddot{\tilde{\mathbf{q}}} + (\mu\mathbf{M}(\mathbf{q}) + \mathbf{C}(\mathbf{q}, \dot{\mathbf{q}}) + \mathbf{D}_d)\dot{\tilde{\mathbf{q}}} \\ + (\mu\mathbf{D}_d + \mu\mathbf{C}(\mathbf{q}, \dot{\mathbf{q}}) + \mathbf{K}_d)\tilde{\mathbf{q}} = \tau_{dist} \end{aligned} \quad (10)$$

Notice that by choosing $\mu = 0$ in equation (10) the closed loop control system is identical to the classical impedance control without inertia shaping of eq. (5).

Remark 1: In case $\|\tilde{\mathbf{q}}\|$ exceeds the predefined upper bound \bar{e} the function $c(\|\tilde{\mathbf{q}}\|)$ exponentially decays to zero implying that the coupling term $kc(\|\tilde{\mathbf{q}}\|)\tilde{\mathbf{q}}$ in eq. (6) is decaying to zero and that the total duration of the desired trajectory $\tau(\|\tilde{\mathbf{q}}\|)$ in eq. (8) increases abruptly pausing the time evolution of the DMP. This implies that $(\mathbf{q}_r, \dot{\mathbf{q}}_r, \ddot{\mathbf{q}}_r) \rightarrow (\mathbf{q}_x, 0, 0)$ with \mathbf{q}_x constant.

IV. STABILITY ANALYSIS

The control system under consideration consists of eq. (6), (10). We claim that this system achieves stable and accurate tracking of the desired trajectory i.e. the actual tracking error $\mathbf{q} - \mathbf{q}_x$ practically converges to zero under the existence of a bounded disturbance input due to model and task uncertainties (i.e. $\tau_{dist} = \tau_e$).

Let us define the error $\mathbf{q}_e = \mathbf{q}_r - \mathbf{q}_x$ between the reference and the desired trajectory and write the DMP system (6) as follows:

$$\begin{aligned} \dot{\mathbf{q}}_e &= \mathbf{z} \\ \dot{\mathbf{z}} &= -d\mathbf{z} - k\mathbf{q}_e - k\tilde{\mathbf{q}} \end{aligned} \quad (11)$$

Further, define the composite error $\mathbf{s} = \dot{\tilde{\mathbf{q}}} + \mu\tilde{\mathbf{q}}$, and write the closed loop robot dynamics of eq. (10) as $\mathbf{M}\dot{\mathbf{s}} + (\mathbf{D}_d + \mathbf{C})\mathbf{s} + \mathbf{K}_d\tilde{\mathbf{q}} = \tau_e$ which in state-space is given by:

$$\begin{aligned} \dot{\tilde{\mathbf{q}}} &= \mathbf{s} - \mu\tilde{\mathbf{q}} \\ \dot{\mathbf{s}} &= -\mathbf{M}^{-1}(\mathbf{D}_d + \mathbf{C})\mathbf{s} - \mathbf{M}^{-1}\mathbf{K}_d\tilde{\mathbf{q}} + \mathbf{M}^{-1}\tau_e \end{aligned} \quad (12)$$

Let us now define the state vector $\boldsymbol{\xi} = [\boldsymbol{\xi}_1^T, \boldsymbol{\xi}_2^T]^T$ with $\boldsymbol{\xi}_1$, $\boldsymbol{\xi}_2$ given by:

$$\boldsymbol{\xi}_1 = [\tilde{\mathbf{q}}^T \quad \mathbf{s}^T]^T, \quad \boldsymbol{\xi}_2 = [\mathbf{q}_e^T \quad \mathbf{z}^T]^T \quad (13)$$

and express (12) and (11) as the following interconnected system:

$$\dot{\boldsymbol{\xi}} = \begin{bmatrix} \mathbf{h}_1(t, \boldsymbol{\xi}_1) + \mathbf{u} \\ \mathbf{h}_2(\boldsymbol{\xi}_2) + \mathbf{g}_2(\boldsymbol{\xi}_1) \end{bmatrix} \quad (14)$$

where $\mathbf{u} = \mathbf{M}^{-1}\tau_e$ and

$$\begin{aligned} \mathbf{h}_1(t, \boldsymbol{\xi}_1) &= \begin{bmatrix} \mathbf{s} - \mu\tilde{\mathbf{q}} \\ -\mathbf{M}^{-1}(\mathbf{D}_d + \mathbf{C})\mathbf{s} - \mathbf{M}^{-1}\mathbf{K}_d\tilde{\mathbf{q}} \end{bmatrix} \\ \mathbf{h}_2(\boldsymbol{\xi}_2) &= \begin{bmatrix} 0 & 1 \\ -k & -d \end{bmatrix} \boldsymbol{\xi}_2, \quad \mathbf{g}_2(\boldsymbol{\xi}_1) = \begin{bmatrix} 0 & 0 \\ -kc(\|\tilde{\mathbf{q}}\|) & 0 \end{bmatrix} \boldsymbol{\xi}_1 \end{aligned} \quad (15)$$

We can now proceed with the proof as follows. First we prove that the unforced system (14) ($\tau_e = 0$) converges to the origin exponentially for arbitrary initial conditions. Then we show that for a bounded disturbance input τ_e the system state $\boldsymbol{\xi}$ remains bounded, which implies that the virtual tracking error $\tilde{\mathbf{q}}$ remains bounded. We then show that the actual tracking error $\mathbf{q} - \mathbf{q}_x$ practically converges to zero with appropriate control parameter selection.

Theorem 1: The interconnected system (14) exhibits the following properties:

- 1) The origin $\boldsymbol{\xi} = 0$ is an exponentially stable equilibrium of the unforced system i.e. ($\mathbf{u} = 0$).
- 2) The system is Input-to-state stable (ISS) for a bounded input $\mathbf{u}(t)$.

Proof: 1) Following the reasoning of [11] we firstly ignore the interconnection term \mathbf{g}_2 in (14) and we study the stability properties of the isolated subsystems \mathbf{h}_1 , \mathbf{h}_2 . Regarding subsystem \mathbf{h}_1 consider the Lyapunov candidate function:

$$V_1(\boldsymbol{\xi}_1, t) = \frac{1}{2}\mathbf{s}^T\mathbf{M}(\mathbf{q})\mathbf{s} + \frac{1}{2}\tilde{\mathbf{q}}^T\mathbf{K}_d\tilde{\mathbf{q}} \quad (16)$$

which satisfies the first condition of Theorem 4.10 (pp. 154 in [11]) for $a = 2$, $k_{11} = \min\{\lambda_{\min}(\mathbf{M}(\mathbf{q})), \lambda_{\min}(\mathbf{K}_d)\}$, $k_{12} = \max\{\lambda_{\max}(\mathbf{M}(\mathbf{q})), \lambda_{\max}(\mathbf{K}_d)\}$. Taking the time derivative of (16) yields:

$$\begin{aligned} \dot{V}_1 &= -\mathbf{s}^T\mathbf{D}_d\mathbf{s} - \mu\tilde{\mathbf{q}}^T\mathbf{K}_d\tilde{\mathbf{q}} \\ &\leq -k_{13}\|\boldsymbol{\xi}_1\|^2 \end{aligned} \quad (17)$$

where we have utilized the well-known property $\dot{\mathbf{M}} - 2\mathbf{C} = 0$, [11]. It is evident that (17) satisfies the second condition of Theorem 4.10 (pp. 154 in [11]) for $a = 2$, $k_{13} = \min\{\lambda_{\min}(\mathbf{D}_d), \mu\lambda_{\min}(\mathbf{K}_d)\}$ proving the exponential stability of $\boldsymbol{\xi}_1 = 0$ for subsystem \mathbf{h}_1 . Notice that the exponential decay rate is given by:

$$\lambda \triangleq \frac{k_3}{k_2a} = \frac{\min\{\lambda_{\min}(\mathbf{D}_d), \mu\lambda_{\min}(\mathbf{K}_d)\}}{2\max\{\lambda_{\max}(\mathbf{M}(\mathbf{q})), \lambda_{\max}(\mathbf{K}_d)\}} \quad (18)$$

which is positive $\forall \mu > 0$ regardless of the choice of the stiffness and damping gains \mathbf{K}_d , \mathbf{D}_d .

Next we turn our attention to the isolated subsystem \mathbf{h}_2 which is a linear system. Therefore, a reasonable Lyapunov candidate is:

$$V_2(\boldsymbol{\xi}_2) = \boldsymbol{\xi}_2^T\mathbf{P}\boldsymbol{\xi}_2 \quad (19)$$

with \mathbf{P} being a symmetric positive definite matrix. By solving the Lyapunov equation for $\mathbf{Q} = \mathbf{I}_6$ with \mathbf{I}_6 being the identity matrix of dimension six we get:

$$\mathbf{P} = \begin{bmatrix} \mathbf{P}_1 & \mathbf{P}_s \\ \mathbf{P}_s & \mathbf{P}_2 \end{bmatrix} \quad (20)$$

with $P_1 = \frac{d^2+k^2+k}{2dk}I_3$, $P_s = \frac{1}{2k}I_3$, $P_2 = \frac{k+1}{2dk}I_3$. Clearly V_2 , \dot{V}_2 fulfill the conditions of Theorem 4.10 (pp. 154 in [11]) for $a = 2$, $k_{21} = \lambda_{\min}(P)$, $k_{22} = \lambda_{\max}(P)$, $k_{23} = 1$ demonstrating the exponential stability of subsystem h_2 . In addition, V_2 satisfies:

$$\left\| \frac{\partial V_2}{\partial \xi_2} \right\| \leq \beta_2 \|\xi_2\| \quad (21)$$

with $\beta_2 = 2\lambda_{\max}(P) > 0$. Moreover, the interconnection term $g_2(\xi_1)$ satisfies the following inequality as it can be clearly deduced from (15):

$$\|g_2(\xi_1)\| \leq \gamma_{21} \|\xi_1\| \quad (22)$$

with $\gamma_{21} = k > 0$ since $c(\|\tilde{q}\|) \in [0, 1]$.

Let us now consider the composite Lyapunov function:

$$V(\xi, t) = d_1 V_1(\xi_1, t) + d_2 V_2(\xi_2) \quad (23)$$

with $d_1, d_2 > 0$. Utilizing the properties (17), (21), (22), its time derivative satisfies:

$$\dot{V} \leq -d_1 k_{13} \|\xi_1\|^2 - d_2 k_{23} \|\xi_2\|^2 + 2d_2 \beta_2 \gamma_{21} \|\xi_1\| \|\xi_2\| \quad (24)$$

which can be written in quadratic form as:

$$\dot{V} \leq -\frac{1}{2} \phi^T (DS + S^T D) \phi \quad (25)$$

with:

$$D = \text{diag}(d_1, d_2) \quad S = \begin{bmatrix} k_{13} & 0 \\ -2\beta_2 \gamma_{21} & k_{23} \end{bmatrix} \quad (26)$$

$$\phi = [\|\xi_1\|, \|\xi_2\|]^T$$

Notice that S is an M -matrix since all its leading principal minors are positive and therefore invoking Lemma 9.7 (pp. 360 of [11]) there exists a positive diagonal matrix D such that $DS + S^T D$ is positive definite. Moreover since:

$$\dot{V} \leq -\frac{1}{2} \lambda_{\min}(DS + S^T D) \|\xi\|^2$$

system (14) fulfills the conditions of Theorem 4.10 (pp. 154 in [11]) for $a = 2$, $k_1 = \min\{d_1 k_{11}, d_2 k_{21}\}$, $k_2 = \max\{d_1 k_{12}, d_2 k_{22}\}$, $k_3 = \frac{1}{2} \lambda_{\min}(DS + S^T D)$ implying exponential convergence to the origin $\xi = 0$.

2) Since the global exponential stability of the origin of the unforced system (i.e. $u = 0$) is proven, input-to-state stability (ISS) follows directly from Lemma 4.6 (pp. 176 of [11]) which completes the proof. ■

Consider now a bounded disturbance input τ_e due to model and task uncertainties acting on the robot. ISS implies that for a bounded disturbance τ_e the state ξ of the system remains bounded, hence \tilde{q} remains bounded. Consider now the impedance control system of eq. (10) with τ_e , \tilde{q} being the input and the output of the system respectively. Since the unforced system is proved to be exponentially stable, initial conditions are exponentially forgotten, thus we can state that the solution trajectory of the forced system with bounded τ_e converges exponentially to a ball around the equilibrium of radius R which satisfies the inequality:

$$\dot{R} + \lambda R \leq a \|\tau_e\| \quad (27)$$

for some positive a and with λ given by eq. (18). The above inequality implies that frequencies larger than λ are filtered out. Hence, the impedance control system (10) acts as a low pass filter on the input τ_e with its bandwidth determined by the stiffness and damping gains K_d , D_d which are selected at low values for compliance, implying that higher frequencies in τ_e are filtered out.

Consider now the second order linear system eq. (11) with \tilde{q} , q_e being its input and output respectively. Its bandwidth is given by $\omega_n = d/2$ which is a tunable parameter. If $\|\tilde{q}\| < \bar{e}$, $c(\|\tilde{q}\|) = 1$ and if the bandwidth of (11) is selected via d to be significantly larger than the bandwidth λ of the impedance control system (10) then the output accurately tracks the input hence $q_e \approx -\tilde{q}$ as the input is not attenuated or shifted significantly for any of its frequency content component. Since $q_e = q_r - q_x$ and $\tilde{q} = q - q_r$ we can conclude that $q - q_x \approx 0$.

V. SIMULATION

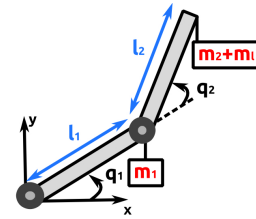


Fig. 2. Planar robot manipulator

Consider a 2-dof robot manipulator with two revolute joints q_1, q_2 and link lengths l_1, l_2 . The masses of the links m_1 and m_2 are considered concentrated at the end of the links and an additional external load of mass m_l has been added on the end effector. The dynamic model of the robot is taken from [12]. Notice that the addition of the extra weight m_l which is considered as a task uncertainty alters the dynamic model of the robot to:

$$M = \hat{M} + M_l \quad C = \hat{C} + C_l \quad g = \hat{g} + g_l \quad (28)$$

with:

$$M_l = \begin{bmatrix} m_l(l_1^2 + 2l_1 l_2 c_2 + l_2^2) & m_l(l_2^2 + l_1 l_2 c_2) \\ m_l(l_2^2 + l_1 l_2 c_2) & m_l l_2^2 \end{bmatrix}$$

$$C_l = \begin{bmatrix} -2m_l l_1 l_2 s_2 \dot{q}_2 & -m_l l_1 l_2 s_2 \dot{q}_2 \\ m_l l_1 l_2 s_2 \dot{q}_1 & 0 \end{bmatrix} \quad (29)$$

$$g_l = \begin{bmatrix} m_l l_1 g c_1 + m_l l_2 g c_{12} \\ m_l l_2 g c_{12} \end{bmatrix}$$

with $c_i = \cos(q_i)$, $s_i = \sin(q_i)$, $c_{ij} = \cos(q_i + q_j)$ and g being the gravity acceleration.

The robot control law is implemented utilizing eq. (9) with the available dynamic model of the robot given in terms of \hat{M} , \hat{C} , \hat{g} from eq. (28). The robot dynamics with the addition of the uncertain load m_l is given by (3),(28) and the disturbance input due to the uncertain load is given by:

$$\tau_e = -M_l \ddot{q}_r - C_l \dot{q}_r - g_l + \mu M_l \dot{\tilde{q}} + \mu C_l \tilde{q} \quad (30)$$

From eq. (18) we can see that the parameter μ determines a lower bound on the exponential convergence rate we are able to guarantee. Larger values of μ enhance the convergence rate but they also increase the apparent stiffness of the modified impedance dynamics as can be seen from eq. (10). For simplicity we choose $\mu < 1$ so that the stiffness component of the modified impedance dynamics is mainly reflected by the gain \mathbf{K}_d . For designing a damping matrix to achieve an approximately critically damped response we follow the procedure proposed in [1] for the classical impedance control without inertia shaping. Specifically the damping matrix is given by [1]:

$$\mathbf{D}_d = 2\mathbf{Q}(\mathbf{q})^T \text{diag}(\zeta_i \sqrt{\lambda_{K,i}^M}) \mathbf{Q}(\mathbf{q}) \quad (31)$$

where ζ_i is a damping factor and $\mathbf{Q}(\mathbf{q})$ is a non singular matrix which satisfies simultaneously $\mathbf{M}(\mathbf{q}) = \mathbf{Q}(\mathbf{q})^T \mathbf{Q}(\mathbf{q})$ and $\mathbf{K}_d = \mathbf{Q}(\mathbf{q})^T \text{diag}(\lambda_{K,i}^M) \mathbf{Q}(\mathbf{q})$ for each particular joint position \mathbf{q} with $\lambda_{K,i}^M$ being the i^{th} generalized eigenvalue of \mathbf{K}_d with respect to $\mathbf{M}(\mathbf{q})$. By selecting $\zeta_i > 1$ we can account for the effect of μ and achieve an approximately critically damped response.

Parameter selection: The parameters of the dynamic model of the robot are set to $m_1 = 1$ kg, $m_2 = 0.5$ kg, $m_l = 0.2$ kg, $l_1 = l_2 = 1$ m and $g = 0.98$ m/s².

For the modified impedance control we selected $\mu = 0.5$ and $\mathbf{K}_d = 13\mathbf{I}_3$ (set to low values for highly compliant robot reactions) while \mathbf{D}_d is set from (31) with $\zeta_i = 1.1$, $i = 1, 2$ for an approximately critically damped response.

The DMP system is implemented using eq. (6), (7), (8) with $d = 100$ so that the bandwidth of the DMP is significantly larger than the bandwidth of the impedance dynamics which was estimated to be approximately $\lambda = 0.25$ and $k = d^2/4$ for critically damped response, with the target duration of the desired movement set to $\tau_d = 10$ sec and for the sigmoid like function parameters set to $\gamma_s = 100$ and $\bar{e} = 0.25$. The DMP is trained with synthetic data which realize a 5th order polynomial trajectory from an initial configuration $\mathbf{q}_0 = [0, 0]^T$ rad towards a target configuration $\mathbf{q}_f = [\frac{\pi}{3}, \frac{\pi}{4}]^T$ rad.

Simulation results: First we examine the proposed control scheme performance under the presence of disturbances due to model and task uncertainties. In Fig. 3 the response of the disturbance input τ_e for each joint is depicted while Figure 4 depicts the responses of the virtual tracking error $\tilde{\mathbf{q}} = \mathbf{q} - \mathbf{q}_r$, the DMP error $\mathbf{q}_e = \mathbf{q}_r - \mathbf{q}_x$ and the actual tracking error $\mathbf{q} - \mathbf{q}_x$ for each joint. Notice that the disturbance input τ_e induces a virtual tracking error $\tilde{\mathbf{q}}$ to the system which is compensated by the DMP generated error \mathbf{q}_e leading the actual tracking error $\mathbf{q} - \mathbf{q}_x$ practically to zero. Figure 5 depicts the robot joint trajectory \mathbf{q} which almost coincide with the desired joint trajectory \mathbf{q}_x as well as the reference joint trajectory \mathbf{q}_r . Notice how the reference joint trajectory \mathbf{q}_r is displaced with respect to the desired trajectory \mathbf{q}_x thus compensating for the errors due to model and task uncertainties. Fig. 6 depicts the error norm responses of $\|\tilde{\mathbf{q}}\|$, $\|\mathbf{q}_e\|$ and $\|\mathbf{q} - \mathbf{q}_x\|$ confirming that the norm of the virtual tracking error $\|\tilde{\mathbf{q}}\|$ matches that

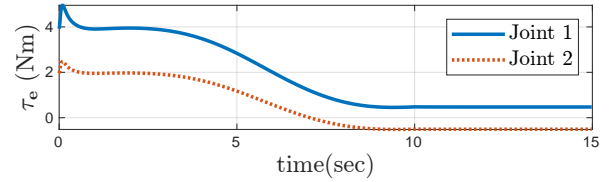


Fig. 3. Torque disturbance input response due to model and task uncertainties for each joint.

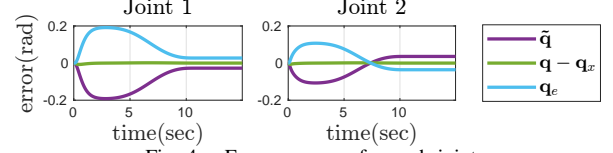


Fig. 4. Error response for each joint.

of the DMP generated error norm $\|\mathbf{q}_e\|$ which is allowed by the fact that $\|\tilde{\mathbf{q}}\|$ does not exceed the predefined threshold \bar{e} , implying that $c(\|\tilde{\mathbf{q}}\|) = 1$. This results in the successful compensation of the virtual tracking error, driving the norm of the actual tracking error $\|\mathbf{q} - \mathbf{q}_x\|$ practically to zero.

Next we demonstrate the behavior of the proposed control system when an unexpected contact occurs during the robot motion to showcase its highly compliant reactions. We simulate again eq. (6),(7),(8), (9), (28), (29),(31) and during the motion we consider a torque to be applied to each robot joint emulating an unexpected collision scenario with a human. The contact torque is given by:

$$\tau_{cont} = -[5, 5]^T \chi_{[t_1, t_2]}(t) \quad (32)$$

with $\chi_{[t_1, t_2]}(t)$ denoting a unit pulse in the interval $[t_1, t_2] = [2, 6]$ sec. The contact unit pulse torque and the disturbance inputs τ_e due to model and task uncertainties during the arm's motion is depicted in Fig. 7. Notice the variation on τ_e with respect to the previous simulation when the contact torque τ_{cont} is applied because the system is compliant and τ_e depends on the robot joint position and velocity. In fact, notice in Figure 8 the increase in the resulting error norm response (Lower plot) when the contact torque is applied with its norm depicted in the upper plot. In particular, the application of the contact torque τ_{cont} leads $\|\tilde{\mathbf{q}}\|$ to exceed the predefined value \bar{e} implying that $c(\|\tilde{\mathbf{q}}\|) \rightarrow 0$, \mathbf{q}_x pauses, \mathbf{q}_r tends to \mathbf{q}_x (see Remark 1) hence leading $\|\mathbf{q}_e\|$ to zero, which in turn means that any error compensation due to τ_e

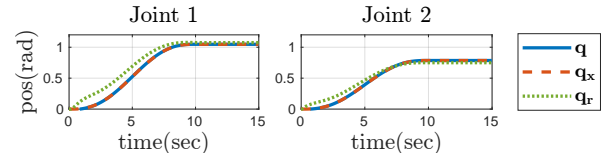


Fig. 5. Joint position response for each joint

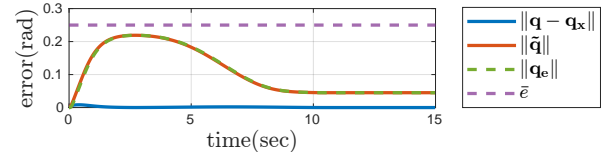


Fig. 6. Error norm response

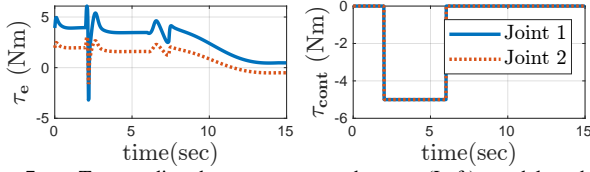


Fig. 7. Torque disturbance response due to: (Left) model and task uncertainties (Right) contact torques for each joint

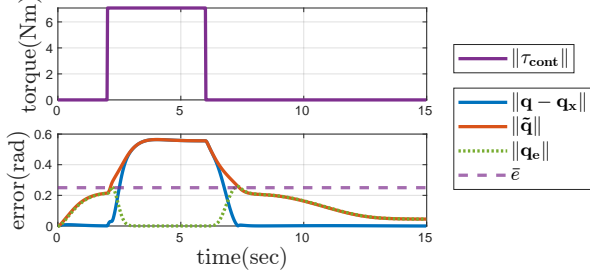


Fig. 8. (Upper) Norm of contact torque response, (Lower) Norm of errors response.

is paused. In this way the robot is able to deviate from the desired trajectory complying with the contact torque as can be seen from the norm of actual tracking error $\|q - q_x\|$ in Fig. 8 and from the robot joint position response q in Fig. 9.

Figure 10 shows the response of the torque control input fed to the robot for both contact and no-contact cases. Notice that the application of a contact torque results in a variation of the control input however it does not exhibit excessive values which could exceed the operation limits of the robot.

Finally a comparison between the proposed approach and the classical impedance control of Section II-B is performed. The stiffness gain of the classical impedance is set to $K_d = 20I_3$ to correspond to the compliance of the proposed approach while D_d is set according to (31) with $\zeta_i = 1$ for critically damped response. In Fig. 11 the norm of the tracking error $\|q - q_x\|$ is depicted (Left) for the contact case and (Right) for the no contact case. Notice that the two approaches exhibit similar compliance to external contact torques however the classical impedance is not able to accurately track the desired trajectory under the presence of model and task uncertainties as opposed to the proposed

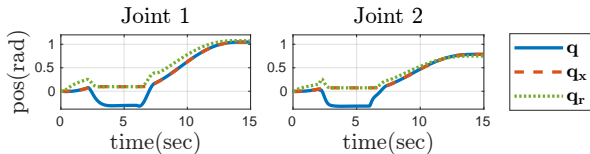


Fig. 9. Joint position response for each joint.

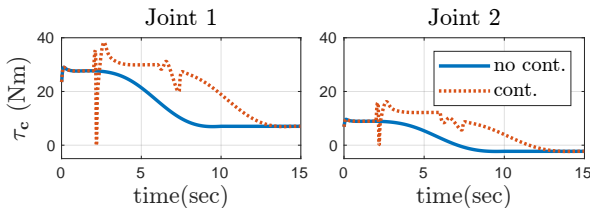


Fig. 10. Robot control input τ_c for each joint with and without contact.

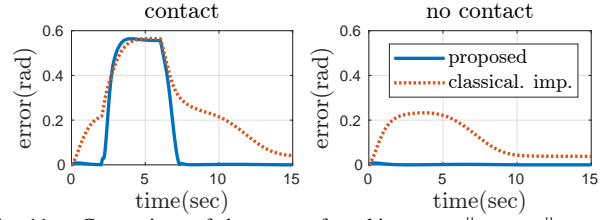


Fig. 11. Comparison of the norm of tracking error $\|q - q_x\|$ response between the proposed control and the classical impedance control (Left) with contact (Right) without contact.

control scheme.

VI. CONCLUSION

This work presented a novel interconnection of a DMP with a modified low impedance controlled robot for accurate tracking and compliant reaction on external forces. The proposed control scheme is analysed theoretically with Lyapunov stability arguments. Simulation results a 2-DOF manipulator demonstrate high tracking accuracy under the presence of model and task uncertainties and highly compliant reactions to external forces arising in unexpected contact events as compared to conventional control approaches. Future work will focus on the experimental validation of the proposed approach in practical scenarios and its formulation on the operational space.

REFERENCES

- [1] C. Ott, "Cartesian impedance control: The rigid body case," in *Cartesian Impedance Control of Redundant and Flexible-Joint Robots*. Springer, 2008, pp. 29–44.
- [2] W. M. Haddad and V. Chellaboina, *Nonlinear Dynamical Systems and Control: A Lyapunov-Based Approach*. NJ, USA: Princeton University Press, 2008.
- [3] G. S. Kanakis and G. A. Rovithakis, "Improving safety in human-robot collaboration via dynamic active constraints enforcement," in *2021 30th IEEE International Conference on Robot & Human Interactive Communication (RO-MAN)*. IEEE, 2021, pp. 515–519.
- [4] F. Ferraguti, C. T. Landi, A. Singletary, H.-C. Lin, A. Ames, C. Secchi, and M. Bonfe, "Safety and efficiency in robotics: The control barrier functions approach," *IEEE Robotics & Automation Magazine*, vol. 29, no. 3, pp. 139–151, 2022.
- [5] K. Kronander and A. Billard, "Stability considerations for variable impedance control," *IEEE Transactions on Robotics*, vol. 32, no. 5, pp. 1298–1305, 2016.
- [6] T. Kastritsi, F. Dimeas, and Z. Doulgeri, "Progressive automation with dmp synchronization and variable stiffness control," *IEEE Robotics and Automation Letters*, vol. 3, no. 4, pp. 3789–3796, 2018.
- [7] K. Vlachos and Z. Doulgeri, "A control scheme with a novel dmp-robot coupling achieving compliance and tracking accuracy under unknown task dynamics and model uncertainties," *IEEE Robotics and Automation Letters*, vol. 5, no. 2, pp. 2310–2316, 2020.
- [8] L. Koutras, K. Vlachos, G. S. Kanakis, F. Dimeas, Z. Doulgeri, and G. A. Rovithakis, "Enforcing constraints for dynamic obstacle avoidance by compliant robots," in *ICRA*, 2023, pp. 5221–5227.
- [9] A. J. Ijspeert, J. Nakanishi, H. Hoffmann, P. Pastor, and S. Schaal, "Dynamical movement primitives: Learning attractor models for motor behaviors," *Neural Computation*, vol. 25, no. 2, pp. 328–373, 2013.
- [10] A. Sidiropoulos and Z. Doulgeri, "A reversible dynamic movement primitive formulation," in *2021 IEEE International Conference on Robotics and Automation (ICRA)*. IEEE, 2021, pp. 3147–3153.
- [11] H. K. Khalil and J. W. Grizzle, *Nonlinear systems*. Prentice hall Upper Saddle River, NJ, 2002, vol. 3.
- [12] J. J. Craig, *Introduction to Robotics: Mechanics and Control*, 3rd ed. Reading, Mass.: Pearson Education / Addison-Wesley, 2005.